$Sr_{1-x}Ag_xTiO_{3\pm\delta}$ (x = 0, 0.1) perovskite-structured catalysts for the flameless combustion of methane

L.Fabbrini[a], A.Kryukov[b], S.Cappelli[a], G.L.Chiarello[a], I.Rossetti[a], C.Oliva[a] and L.Forni[a]*

[a] Dipartimento di Chimica Fisica ed Elettrochimica, Università di Milano
via C.Golgi, 19 I-20133 Milano, Italy
[b] D.I.Mendeleev University of Chemical Technology of Russia, Moscow, Russia

ABSTRACT

Several samples of $Sr_{1-x}Ag_xTiO_{3\pm\delta}$ (x = 0, 0.1) perovskite-structured catalysts have been prepared and tested for the title reaction under lean-burn conditions. For the same overall nominal composition, catalyst activity and durability depend strongly on the method of preparation and, for the samples prepared by the same method, mainly on temperature and on residence time at such a temperature during preparation. In $Sr_{0.9}Ag_{0.1}TiO_{3\pm\delta}$ catalysts Ag is present either as intra-crystalline Ag^{2+}, likely substituting for Sr^{2+} in the perovskite lattice, or as inter-crystalline metallic Ag. The catalytic activity of $Sr_{0.9}Ag_{0.1}TiO_{3\pm\delta}$ is connected with the presence of O_2^-/Ti^{4+}, O_x^-/Ag and O_x^-/Ag^{2+} or of O_3^-/Ti^{4+}, O^-/Sr^{2+} and of O^-/Ti^{4+} species, depending on preparation method and conditions. Furthermore, inter-crystalline metallic Ag plays an important role in improving catalyst resistance to sintering, the most durable samples being those calcined for a sufficient residence time at the highest temperature during preparation, *i.e.* under conditions better favouring the segregation of this metal from the perovskite lattice.

Keywords: Perovskite-structured mixed oxides; Sr-Titanate and Ag-doped Sr-Titanate; Catalytic flameless combustion of methane.

*) Corresponding author. e-mail address: lucio.forni@unimi.it Fax No.: +39-02-50314300

INTRODUCTION

The catalytic flameless combustion (CFC) of hydrocarbons represents the most efficient way for exploiting the chemical energy of hydrocarbons by oxidation of fuel/air lean mixtures, while substantially reducing or even virtually suppressing any formation of NO_x [1-3]. Indeed, at low temperature nitrogen oxides are thermodynamically unstable and hence they cannot form during combustion. Then, provided the combustion is carried out at sufficiently low temperature (<800°C), any need of post-combustion NO_x abatement is removed. The efficiency of noble metals, especially of Pt, as catalysts for the CFC of hydrocarbons is well known since the pioneering work of Faraday and Davy [4] and these metals are still extensively studied [5] for the present reaction, due to the increasingly severe restrictions imposed to improve the quality of air. However, the booming price of noble metals, due to the enormously growing demand during the last three decades, stimulated an intensive research for low-cost substitutes of these catalysts. Among the various potential substitutes, some classes of transition metal oxides mixtures, especially of perovskite-like structure, showed very promising [6,7].

Several kinds of mixed oxides have been prepared and tested by our research group since the late nineties, by using the CFC of methane as test reaction and focusing particularly on $A_{1-x}A'_xBO_3$ (A = La, Sr; A' = Ce, Eu, Sr; B = Co, Mn, Fe, Ni) perovskite-structured oxides [8-17]. During this work, besides employing the traditional calcination-milling [18] and sol-gel-citrates (SGC) [19] methods, an innovative flame hydrolysis (FH) preparation procedure has been proposed by us [11] and, more recently, also the flame-spray pyrolysis (FP) method [20,21] is being applied. Furthermore, an extensive study has been carried out in our laboratory on the anchoring of the same catalysts on a cordierite honeycomb monolith support, through a proper primer, *i.e.* on preparing the catalyst in the form usually selected for practical application [16,17].

Among the most recently tested catalysts, $SrTiO_3$ showed very active for the CFC of methane [22] and its activity was found to further improve when Ag was partially substituted for Sr. This prompted us to the present deeper investigation on these Sr-Titanate and Ag-Sr-Titanate catalysts, aiming at correlating their performance with their physical-chemical characteristics. Furthermore, since the durability of any catalyst for the present reaction represents a particularly important feature for practical application, special attention was paid also on catalyst resistance to decaying.

EXPERIMENTAL

Catalysts preparation

A first set of catalysts was prepared by the SGC technique. However, a particular procedure [23] was needed for the present materials, due to the sensitivity of Ti^{4+} ion to water, causing the immediate precipitation of TiO_2. Briefly, 5 cm^3 of Ti-iso-propoxide (FLUKA, purum) were dropped very slowly into 50 cm^3 of vigorously stirred distilled water. To the so obtained suspension of freshly precipitated $TiO_2 \cdot xH_2O$, 3 mol of citric acid (FLUKA, 99.5% pure) were added per 2 mol of Ti ions, followed by a few cm^3 of hydrogen peroxide (ALDRICH, 30 vol% aqueous solution), till the complete dissolution of the precipitate. A stoichiometric amount of Sr^{2+} ions was then added, from a solution prepared by dissolving $Sr(CH_3COO)_2$ (ACROS, >99% pure) in the minimum of distilled water and adding citric acid so to have an acid/Sr = 1/3 molar ratio. The complexation of metallic ions by citric acid prevented any re-precipitation of TiO_2. The perfectly clear final solution was evaporated *in vacuo* (residual pressure 70 Torr, 1 Torr = 133 Pa) at 35-40°C in rotavapor, till the formation of the gel and then at 70°C till the formation of a yellow coloured powder. The latter was divided into two portions, calcined in flowing air (50 cm^3/min) under different conditions. The first batch while increasing temperature by 0.5°C/min from 25 to 250°C,

maintained for 1 min, and then by 1°C/min up to 950°C, maintained for 60 min. The second batch while increasing temperature by 0.5°C/min from 25 to 250°C, maintained for 1 min, and then by 3°C/min up to 850°C, maintained for 60 min. The two catalysts so obtained are referred to as SGC-1 and SGC-3 (Table 1), respectively.

A second set of catalysts was prepared by slowly dropping directly the Ti-iso-propoxide into a vigorously stirred aqueous solution of citric acid (acid/Ti = 2/1 molar ratio). The fresh $TiO_2 \cdot xH_2O$ precipitate rapidly dissolved by adding a few cm^3 of the previously mentioned hydrogen peroxide solution. To the clear, orange coloured solution so obtained a solution of Ag- nitrate and Sr-acetate was added, prepared by dissolving $AgNO_3$ (Carlo Erba, 99.8% pure) and $Sr(CH_3COO)_2$ in the minimum of water and then adding citric acid in 2/1 molar ratio, with respect to the sum of Ag^+ and Sr^{2+} ions. The perfectly clear final solution was evaporated in rotavapor as previously described and the powder obtained was divided into three portions, calcined in 50 cm^3/min flowing air as follows: after a first step with increasing temperature by 0.5°C/min from 25 to 250°C, maintained for 1 min for each sample, the temperature was increased up to 850°C, then maintained for 60 min. The temperature increasing rate of the second heating step was 1, 2.5 and 5°C/min, respectively, for the three batches. These three catalysts are referred to as AgSGC-1, AgSGC-2.5 and AgSGC-5, respectively (Table 1).

A further sample, named AgFH (Table 1), was prepared by the FH technique. This was described in detail elsewhere [11]. Briefly, a diluted (3 wt %) aqueous solution, prepared as described (*vide supra*) and containing citric acid and the Sr, Ti and Ag ions in the desired ratios, was nebulised in a H_2-O_2 flame. At the high temperature (≥1600°C) of the flame the solvent vaporises instantaneously and the perovskite-structured oxide mixture forms in spheroidal nanoparticles, collected by means of an electrostatic precipitator.

A final couple of catalysts (FP and AgFP, respectively, Table 1) was prepared by the FP method. The procedure has been extensively described elsewhere [20,21]. Briefly, solutions of $Sr(NO_3)_2$, dissolved in propionic acid, of Ti-isopropoxide, dissolved in 2-ethyl-hexanoic acid, and, when required, of $AgNO_3$, dissolved in acetonitrile, were combined in the desired ratios and so to have a 0.05 M overall concentration of the metallic ions. The combined solution was then fed by means of a syringe pump (HARVARD 975) to a capillary tube (1 mm OD, 0.6 mm ID), ending in the centre of a vertical nozzle, 1.1 mm in diameter, to which a constant flow of oxygen (SIAD, purity grade 4.0) was fed. The flame was started and kept stable by a ring of premixed O_2-CH_4 flamelets surrounding the main nozzle. The organic solution sprayed within the oxygen jet of the nozzle instantaneously vaporises and ignites, ending into a spheroidal nanoparticles powder of the oxide mixture, collected by means of the previously mentioned electrostatic precipitator.

Some relevant characteristics of the catalysts prepared and investigated are collected in Table 1.

Catalysts characterisation

Recognition and purity degree of the solid phases were determined by X-ray diffraction (XRD) analysis, by means of a PHILIPS PW1820 powder diffractometer, operated at 40 kV and 40 mA and by employing the Ni-filtered, Cu Kα radiation (λ = 1.5418 Å). The oxides particle size and shape were determined by scanning electron microscopy (SEM), by means of either a CAMBRIDGE STEREOSCAN 150 or a LEICA LEO 1430 instrument. Specific BET surface area (S_{BET}) was measured by nitrogen adsorption-desorption at the liquid nitrogen temperature, by a MICROMERITICS ASAP 2010 instrument. Electron paramagnetic resonance (EPR) spectra were collected by a BRUKER ELEXSYS instrument, equipped with a standard rectangular ER4102ST cavity and operated at 9.4 GHz, 1 mW microwave energy, 1 Gauss modulating amplitude and in

the temperature range between –173 and 25°C. The intensity of magnetic field was carefully checked by a BRUKER ER35M teslameter and the microwave frequency was measured by an HP 5340A frequency meter.

Catalytic activity and thermal stability tests

Catalytic activity comparison tests have been carried out under rigorously standard experimental conditions (*vide infra*) by means of a bench scale apparatus, centred on a continuous, tubular, down-flow, 0.7 cm ID, 40 cm long, quartz reactor. Every run was performed by diluting in 1.3 g of 60-100 mesh quartz powder 0.2 g of catalyst, prepared by pressing (3 tons/cm^2) the original nanoparticle powder into wafers, then crushed and sieved to 60-100 mesh particles. The catalyst bed was kept in the middle, isothermal portion of the reactor tube by small flocks of quartz wool and the void space above and below the catalyst bed was filled with 10-20 mesh quartz beads. The reactor was heated by an electric furnace, controlled by an EUROTHERM 812 TRC, governed by a thermocouple fitted within the heavy metal blocks surrounding the reactor tube. Before the reaction the catalyst was activated *in situ* in 20 cm^3/min flowing air, while increasing temperature by 10°C/min up to 650°C, kept for 1 h. After lowering temperature down to 250°C, the gas flow was switched to a 20 cm^3/min gas mixture composed of 10 cm^3/min of 1.04 vol % CH_4 in He (SIAD, certified mixture) and 10 cm^3/min of air (SIAD, purity grade 5.0) and the test run was immediately started while increasing temperature by 2.3°C/min up to the temperature (T_f) of CH_4 full conversion. The selected value of time factor $\tau = W/F$, W being the catalyst weight (g) and F (cm^3/min) the overall gas flow rate, then resulted 0.6 $g_{cat}s/cm^3_{flowing\ gas}$ for every test run. During any of the runs conversion of CH_4 was monitored every 10 min through gas chromatographic analysis of the outlet gas, carried out by means of an on-line HP 5890 instrument, equipped with thermal conductivity

detector and with two 1/8” OD 2 m long columns in series, packed with Porapak Q and MS-5A, respectively.

The thermal stability accelerated tests were carried out at the end of the standard test runs, by keeping temperature at T_f and checking methane conversion after 100 h on-stream. Then the catalyst was subjected to several overheating/reaction cycles, consisting in increasing temperature by 10°/min up to 800°C, kept for 1 h and then decreasing down to T_f for at least 0.5 h before checking again methane conversion. Neither oxidation products different from CO_2 nor traces of nitrogen oxides of any composition were ever detected in the out coming gas, for any of both activity comparison and thermal stability test runs.

RESULTS AND DISCUSSION

Catalysts characterisation

S_{BET} of the various catalysts is given in Table 1. It may be noticed that the value of this parameter depends strongly on the method of preparation and, for the samples prepared by the same method, also on composition and mainly on residence time and temperature attained during preparation. The higher the latter two parameters, the more sintered became the sample. Indeed, SGC-1, calcined for 2 h at 950°C showed a very small value (1 m^2/g) of S_{BET}, while for SGC-3, AgSGC-1, AgSGC-2.5, and AgSGC-5, calcined for 1 h at a temperature 100°C lower only, values of S_{BET} ranging from 21 to 28 m^2/g were obtained. For the AgFH sample, prepared at very high flame temperature (≥1600°C), but with a very short residence time (of the order of 1 ms), S_{BET} attained 12 m^2/g. On the other hand, values of S_{BET} up to one order of magnitude higher were obtained with the samples prepared by the FP technique, *i.e.* with a similarly short residence time, but with a lower flame temperature (≅1400°C), due to the lower heat of

combustion of the organic solvents employed, with respect to pure hydrogen. Furthermore, among the Ag-doped SGC samples, a small increase of S_{BET} can be noticed when increasing the rate of temperature growth during calcination, likely due to an increasing structural disorder of the solid, conferred by the progressively increasing heating rate.

The XRD patterns of the various catalysts are collected in Fig.1. All of them showed to possess the perovskite-like structure [24]. For the Ag-doped samples this was accompanied by more or less weak peaks at 2θ = 38.2, 44.5, 64.5 degrees, characteristic of the metallic Ag fcc phase [25]. Indeed, all the Ag-doped samples, irrespective of the preparation procedure, showed a more or less faint violet hue, characteristic of the basically white Ag-containing compounds, in which Ag ions partially reduce to metal, which then segregates from the main phase. Furthermore, by comparing the enlarged XRD patterns of the Ag-doped samples, prepared on one hand by the FH and FP procedures and, on the other hand, by the SGC technique, a difference in 2θ up to 0.25 degrees was noticed for the same reflection (see *e.g.* Fig.2, upper part), with respect to the undoped catalyst. The shifting is perfectly confirmed by the main reflection at $2\theta > 50°$ (Fig.2, lower part). This indicates that Sr^{2+} (ionic radius 1.13 Å) has been partially substituted by Ag^{2+} (ionic radius 1.08 Å), so that the cell volume became smaller, causing the shift of the XRD reflection peaks to higher 2θ values, in line with the so called Vegard generalisation. In addition, Fig.2 shows also that a much lower degree of Ag^{2+} substitution for Sr^{2+} in the perovskite lattice has occurred for AgFH and AgFP samples, with respect to AgSGC ones. Indeed, a calculation, relative to the latter samples, showed that most of Ag (*e.g*. up to 60% of the nominal amount for the AgSGC-1 sample) was present as intra-crystalline, framework Ag^{2+} in the perovskitic lattice. This is very likely a consequence of the less severe SGC preparation conditions experienced by the solid, with respect to either FH or FP method, allowing the perovskitic lattice of the AgSGC sample to allocate a higher amount of extraneous ions. As a vicar of the Sr^{2+} ion, the lattice Ag^{2+} ion is forced to

assume this unusual charge by the perovskite crystal field force. Due to the difference in ionic radii (*vide supra*), the perovskitic structure however permits to accommodate such ions within a rather low substitution degree only, depending on the method of preparation. Due to the high-temperature instability of Ag oxides and the relatively low melting point of metallic silver, it cannot be excluded that a part of silver was lost during high-temperature synthesis (FH and FP techniques). Furthermore, some Ag is segregated in metallic extraframework form, as evidenced by XRD analysis. Hence, sample composition of Table 1 have to be considered as indicative only.

SEM micrographs (Fig.3) showed that all the catalysts were composed of spheroidal nanoparticles. The size of the latter was larger for the samples prepared by the SGC method (up to 100 nm) and especially by the FH technique (up to 800 nm), and smaller (30-60 nm) for those prepared through the FP method. This is roughly in line with the different values of S_{BET} of the various catalysts (Table 1). Since the higher the average particle size, the lower was the S_{BET} value, this means that total specific surface area was essentially due to the external surface of the nanoparticles, the latter being substantially non porous.

Further information about the nature of the species catalytically active for the CFC of methane and about the valence of Ag ions and/or the possible presence of metallic Ag in our Ag-doped samples was collected through the EPR analysis. For the $SrTiO_{3\pm\delta}$ samples, in a previous paper [22] it has been shown that the presence of species more or less active for the present reaction depends on the catalyst preparation procedure. Indeed, in a catalyst prepared by the FH technique both the O_3^-/Ti^{4+} and O^-/Ti^{4+} couples were found in a relatively high amount, while in a sample prepared by the same technique, but employing a different complexing agent (tartaric instead of citric acid) a greater amount of several O^-/Ti^{4+} species was found, accompanied by some increase of catalytic activity. In

addition, the FH technique only led to a substantial formation of these species, the SGC technique leading to samples in which titanium was present prevalently as Ti^{3+} ion.

Many papers in literature deal with O_2^- ions adsorbed on oxides surface or interacting with cations in many systems [26]. Particularly, Känzig and Cohen [27] derived a set of three equations for the *g* values of O_2^- ions involved in purely ionic interactions. These equations are based on the absolute value (152 cm^{-1}) of the oxygen spin-orbit interaction constant λ and on the Δ and *E* splittings of the energy levels for the same O_2^- species in the presence of a crystal field (Fig.4). The lowest value of g_{xx}, calculated through these equations is almost always very close to the value g_e of the free electron [28-33] and this was confirmed also by us for the O_2^-/Ti^{4+} species in $SrTiO_{3\pm\delta}$ [22].

For the present AgFH sample, the EPR spectrum could be fitted, through the BRUKER SimFonia programme (Fig.5), with g_{xx} = 2.007, a value rather too high with respect to that (2.0021) calculated through the mentioned equations. However, a shift of the same order of magnitude for the g_{xx} value has been frequently reported and attributed either to coupling of O_2^- with the *f*-electrons of the metal cation [34-38], or to the presence of not completely ionic bonds [39,40], for which those equations cannot be considered completely valid any more. Therefore, since virtually no trace of the Ag^{2+} pattern (*vide infra*) was noticed in the EPR spectrum of the present AgFH sample (Fig.5), while the presence of metallic Ag was shown by the XRD analysis (Fig.1), we can conclude that O_x^-/Ag couples would be present in this catalyst, similar to what reported for O_2^- adsorbed on metallic Ag in other systems [40,41].

Furthermore, in Fig.5 some lines can be observed in the EPR spectrum of AgFP, perfectly coinciding with those found with the FP sample (here not shown) and with those found in a $SrTiO_{3\pm\delta}$ sample ([22] there labelled with T1), prepared by the FH procedure. Those lines were attributed to O_3^-/Ti^{4+}, to O^-/Sr^{2+} and to different O^-/Ti^{4+} species leading to a higher activity of that catalyst [22].

In addition, the EPR spectra of the AgSGC-1 and AgSGC-5 catalysts are compared in Fig.6. They are identical, except for intensity, which is 6 times lower for the latter catalyst, with respect to the former. These spectra can be unambiguously attributed to $4d^9$ Ag^{2+} ions, though the EPR evidence of them does not exclude the simultaneous presence of Ag^{+} ions.

Indeed, no paramagnetic species other than Ag^{2+} can be hypothesized [42] to account for this EPR pattern. Though relatively few papers only have been published up to date on Ag^{2+} species, due to the difficult stabilisation of such an oxidation state, an EPR spectrum practically identical to those of Fig.6 has been observed since 1961 with Ag^{2+} in frozen solutions of HNO_3 or H_2SO_4 [43]. Ag^{2+} EPR spectra of this kind have been reported also with $Ag(SO_3F)_2$ [44,45], with $AgMF_6$ (M = Sn, Pb, Hf, Zr) and with $MAgF_4$ (M = Ba, Ca, Hg, Sr), in which Ag^{2+} centres were in either axially elongated tetragonal or in square-planar arrangements [46,47]. At last, spectra like these have been reported with many solid state systems after γ-irradiation and attributed to Ag^{2+}. Among them, single crystals of $Ca(OD)_2$:Ag [48] and of $CdCl_2$:Ag [49], as well as AgX zeolites [50] may be cited. In the present case, the $4d^9$ Ag^{2+} electron resides in the d_{x2-y2} orbital embedded in a tetragonally elongated octahedral crystal, as indicated by the fact that $g_{//} > g_{\perp}$ [42,51].

We propose that Ag^{2+} substitutes for Sr^{2+} in the perovskitic structure, though the only compound known up to date in Ag-Ti-O ternary system is Ag_2TiO_3 [52]. Indeed, if Ag^{2+} would be present as extra-framework AgO impurity, it would not contribute to the EPR pattern, because the latter contains alternating Ag^{+} and Ag^{3+} ions, leading to a diamagnetic system [53]. In any case, the presence of any other extra-framework Ag^{2+}-containing impurities contributing to the EPR pattern seems very unlikely, because the EPR spectrum did not change after leaching the sample with nitric acid (*vide infra*). Furthermore, our XRD pattern (Fig.1) excludes the presence of any other Ag containing phase, apart from traces of metallic Ag. Moreover, the substitution of Ag^{2+} (ionic radius

1.08 Å) for Sr^{2+} (ionic radius 1.13 Å) is in agreement with the above mentioned decreasing of cell volume evidenced by XRD (Fig.2). Such Ag^{2+} ions could interact with some O_x^- species, leading to O_x^-/Ag^{2+} couples. The nature of these O_x^- species is now under investigation.

At last, the presence of Ag^{2+} ions can be hardly observed in AgFP and virtually excluded in AgFH EPR patterns (Fig.5), further in line with the results of the XRD analysis (Fig.2), which suggest a much more pronounced partial substitution of Ag^{2+} for Sr^{2+} in the AgSGC samples.

Catalytic activity

The results of catalytic activity comparison tests for the present catalysts are shown in Fig.7. No relation was observed between catalytic activity and intensity of the Ti^{3+} EPR line (Fig.5). Therefore, this species seems not involved in the reaction. The superior performance of the Ag-doped *vs.* undoped SGC catalysts is immediately evident. Indeed, the former lead to full conversion of CH_4 at $T_f < 570°C$, while for the latter a T_f higher than 610°C is needed to attain the same result. In principle the higher catalytic activity of the Ag-doped samples could be due to the presence of either metallic Ag, as suggested in some previous papers [54,55], or of Ag^{2+}-containing species, or of neither of them. Instead, it can be due to the presence of a higher concentration of oxygen-based species. Aiming at verifying the first of these hypotheses, the AgSGC-2.5 sample was repeatedly treated with a 4 wt % nitric acid solution, to oxidise and leach away most of the metallic Ag. The XRD analysis of the solid, recovered after rinsing and drying overnight at 100°C the so treated catalyst, referred to as AgSGC-2.5R, showed a neat decrease of the weak pattern due to metallic Ag. This was accompanied by the appearance of Ag^+ ions in the nitric leaching solution, confirmed through the usual precipitation of the corresponding amount of AgI after addition of a KI solution. Furthermore, the EPR spectra of AgSGC-2.5

and AgSGC-2.5R showed an almost identical concentration of Ag^{2+} (Fig.8), showing that the nitric acid treatment practically unaffected the Ag^{2+} species. In addition, the conversion *vs.* temperature curves of the activity tests carried out on the AgSGC-2.5 and AgSGC-2.5R samples perfectly overlapped (Fig.9). Therefore, the role of the metallic Ag in the catalytic activity can be ruled out. Then, the higher activity of the SGC-prepared Ag-doped catalysts, with respect to the undoped ones, could be connected with the presence of the Ag^{2+}-based species. However, AgSGC-5 showed more active than AgSGC-1 (Fig.7) though the Ag^{2+} EPR spectrum was less intense with the former than with the latter (Fig.6). Therefore, also the concentration of Ag^{2+} species seems not directly related to the catalytic activity of these samples. Furthermore, the different activity (T_f ranging from *ca*. 502 to *ca*. 569°C, Fig.7) of the three AgSGC samples should be connected with the different concentration of oxygen-based species, which in turn seem directly connected with the degree of disorder inferred by the different rate of temperature increasing during preparation. In fact, the curves of AgSGC-2.5 and AgSGC-1 are progressively shifted, with T_f values of 550 and 570°C, respectively.

A parallel behaviour can be noticed when comparing the activity of Ag-doped catalysts prepared by different methods (Fig.7). The activity curves of AgFP and AgSGC-5 are almost perfectly overlapping, with T_f values of *ca*. 505°C for both of them. This is in line with the observation that many oxygen-based species appear also in the EPR spectrum of AgFP, at difference with AgFH (Fig.5), which showed the worst-performing catalyst of the set, with $T_f \cong 650$°C. One may conclude that the O_x^-/Ag^{2+}-based species present in the AgSGC are characterised by catalytic activity comparable to that of the O_3^-/Ti^{4+}, O^-/Sr^{2+} and of O^-/Ti^{4+} species detected in AgFP by the EPR analysis. By contrast, the O_x^-/Ag^{2+}-based species appear much more active than the O_x^-/Ag-based species present in AgFH (Fig.5).

Thermal stability

The comparison of the thermal stability tests data are reported in Fig.10-12, for the catalysts prepared by the FP, FH and SGC methods, respectively. It may be observed that in any case Ag doping improves significantly the stability of the catalyst, the CH_4 conversion data after several accelerated deactivation-reaction cycles being always much better for the Ag-doped samples. However, a noticeable difference in the resistance to high temperature treatment is conferred by the three preparation procedures here tested.

The catalysts prepared by the FP method (Fig.10) proved the less resistant. Indeed, the AgFP sample appeared rather stable after 100 h on-stream, but, after the first deactivation-reaction cycle, CH_4 conversion dropped to 82%, further dropping to 75% after the third cycle. Deactivation rate was much more pronounced for the FP sample, for which conversion hardly attained 80% after 100 h on-stream and dropped to 42% after the first deactivation-reaction cycle only.

The catalysts prepared by the FH method proved the most resistant (Fig.11). The FH sample showed a CH_4 conversion of 98% after 100 h on-stream and of over 91% after the third deactivation-reaction cycle, while the AgFH showed to attain a CH_4 conversion of 98.5% after the third deactivation-reaction cycle.

As for the catalysts prepared by the SGC method (Fig.12), the best-performing sample was AgSGC-1, showing a CH_4 conversion of over 99% after the third deactivation-reaction cycle. A similar behaviour was shown by AgSGC-2.5. In spite of a small decreasing of conversion (96.5%) after 25 h on-stream only, its activity decayed very slowly, ensuring a 93% conversion after the third deactivation-reaction cycle. When further increasing the rate of temperature increasing during preparation (AgSGC-5 sample), activity increased (Fig.7), but at the expenses of a lower thermal stability (Fig.12). Indeed, while remaining rather stable after 100 h-on-stream, partly due also to the relatively low value of T_f (502°C), conversion dropped to 83% after the third deactivation-reaction cycle.

As evidenced by EPR and XRD analysis (*vide supra*), the higher the rate of temperature increasing during preparation, the lower was the concentration of intra-crystalline Ag^{2+} and the higher the amount of inter-particle metallic Ag in the catalyst. The latter confers a better resistance to sintering to the perovskite nanoparticles, by keeping them better separated from each other. At last, also in this case the worst catalyst showed the undoped sample (SGC-3). Indeed, in spite of a rather slow deactivation rate, similar to that of AgSGC-5, during the first 100 h on-stream, conversion dropped to 77% after the third deactivation-reaction cycle.

A further test was finally carried out with the AgSGC-2.5R catalyst, aiming at checking the effect of nitric acid treatment on thermal stability. In spite activity showed practically unaffected by such a treatment (Fig.9), thermal stability was rather poor (Fig.13). In fact, the CH_4 conversion decreased considerably even after 24 h on-stream and further dropped drastically after the first deactivation-reaction cycle only. This further confirms the protective action of inter-particle Ag against perovskite sintering.

CONCLUSIONS

Perovskite-structured $SrTiO_{3\pm\delta}$, and especially $Sr_{0.9}Ag_{0.1}TiO_{3\pm\delta}$, confirm among the best substitutes of noble-metal-based catalysts for the CFC of methane under lean-burn conditions. For the same overall nominal composition, catalyst activity and durability depend strongly on the method of preparation. Indeed, for the samples prepared by the same method, a longer residence time at a given temperature during preparation entrains a higher durability, but a lower catalytic activity. In $Sr_{0.9}Ag_{0.1}TiO_{3\pm\delta}$ catalysts Ag is present either as intra-crystalline Ag^{2+}, likely substituting for Sr^{2+} in the perovskite lattice, or as inter-crystalline metallic Ag. However, the catalytic activity of these samples is not directly related to these Ag species, but to the presence of O^-/Ti^{4+}, O_2^-/Ti^{4+}, O_3^-/Ti^{4+}, O^-/Sr^{2+} and of

O_x^-/Ag^{2+} or O_x^-/Ag, the last being less active than the other. Furthermore, inter-crystalline metallic Ag plays an important role in improving catalyst resistance to sintering, the most durable catalysts being those calcined for a sufficient residence time at the highest temperature during preparation, *i.e.* under conditions better favouring the segregation of this metal from the perovskite lattice.

AKNOWLEDGEMENTS

The valuable help of Dr. M. Scavini for interpretation of XRD patterns is gratefully acknowledged.

REFERENCES

1. M.F.Zwinkels, S.G.Järås, P.G.Menon, Catal. Rev. Sci. Eng., 25 (1993) 319.
2. H.Arai, M.Machida, Catal. Today, 10 (1991) 81.
3. K.Eguchi, H.Arai, Catal. Today, 29 (1996) 379.
4. H. Davy, in “The Collected Works of Sir Humphrey Davy” (J. Davy, Ed.), Smith, Elder and Co., Cornhill, London, 1840, vol. 6.
5. J. Arbiol, A. Cabot, J. R. Morante, F. Chen, M. Liu, Appl. Phys. Lett., 81, (2002) 3449.
6. J.L.G. Fierro, in “Properties and applications of Perovskite-Type Oxides”, (L.G.Tejuca and J.L.G.Fierro, Eds.), Dekker, New York, 1993.
7. M.A. Peña, J.L.G. Fierro, Chem. Rev., 101 (2001) 1981.
8. L.Marchetti, L.Forni, Appl. Catal., B: Environmental, 15 (1998) 179.
9. D.Ferri, L.Forni, Appl. Catal., B: Environmental, 16 (1998) 119.
10. C.Oliva, L.Forni, Appl. Magn. Res., 18 (2000) 475.
11. R.A.M.Giacomuzzi, M.Portinari, I.Rossetti, L.Forni, Stud. Surf. Sci. Catal. (A.Corma, F.V.Melo, S.Mendioroz, J.L.G.Fierro, Eds.), vol. 130, Elsevier, Amsterdam, 2000, p.197.

12. R.Leanza, I.Rossetti, L.Fabbrini, C.Oliva, L.Forni, Appl. Catal., B: Environmental, 28 (2000) 55.
13. C.Oliva, L.Forni, A.D'Ambrosio, F.Navarrini, A.D.Stepanov, Z.D.Kagramanov, A.I.Mikhailichenko, Appl. Catal., A: General, 205 (2001) 245.
14. I.Rossetti, L.Forni, Appl.Catal., B: Environmental, 33 (2001) 345.
15. L.Forni, I.Rossetti, Appl. Catal., B: Environmental, 38 (2002) 29.
16. L.Fabbrini, I.Rossetti, L.Forni, Appl. Catal., B: Environmental, 44 (2003) 107.
17. L.Fabbrini, I.Rossetti, L.Forni, Appl. Catal., B: Environmental, in press.
18. M.G.S. Baythoun, F.R.Sale, J. Mater. Sci., 17 (1982) 2757.
19. H.M. Zhang, Y. Teraoka, N. Yamazoe, Chem. Lett. 1 (1987) 665.
20. L. Mädler, H. Kammler, R. Mueller, S. Pratsinis. Aerosol Science, 33 (2002), 369.
21. R. Strobel, L. Mädler, W.J. Stark, S. E. Pratsinis, A. Baiker. J. Catal. 213 (2003), 296.
22. C.Oliva, L.Bonoldi, S.Cappelli, L.Fabbrini, I.Rossetti, L.Forni, J.Molec.Catal., A: Chemical, 226 (2005) 33.
23. R.N.Das, P.Pramanik, Brit. Ceram. Trans., 99 (2000) 153.
24. Selected Powder Diffraction Data, JCPDS, Swarthmore, PA, file 5-418.
25. Selected Powder Diffraction Data, JCPDS, Swarthmore, PA, file 01-1167.
26. M. Che, A.J. Tench, in "Advances in Catalysis", (D.D.Eley, H.Pines and P.B.Weisz, Eds.), Academic Press, San Diego, 1983, vol.32, p.1.
27. W. Känzig, M.H. Cohen, Phys. Rev. Lett., 3 (1959) 509.
28. A. Tuel, J. Diab, P. Gelin, M. Dufaux, J.-F. Dutel, Y, Ben Taarit, J. Molec. Catal., 63 (1990) 95.
29. C. Louis, T. Lin Chang, M. Kermarec, T. Le Van, J.M. Tatibouet, M. Che, Coll. and Surf., A: Physicochem. and Engineering Aspects, 72 (1993) 217.
30. T. Yang, L. Feng, S. Shen, J. Catal., 145 (1994) 384.
31. K. Dyrek, A. Adamski, Z. Sojka, Spectrochimica Acta, Part A, 54 (1998) 2337.

32. A.L. Attwood, D.M. Murphy, J.L. Edwards, T.A. Egerton, R.W. Harrison, Res. Chem. Intermed. 29 (2003) 449.
33. A.L. Attwood, J.L. Edwards, Ch.C. Rowlands, D.M. Murphy, J. Phys. Chem., 107 (2003) 1779.
34. M. Setaka, T. Kwan, Bull. Chem. Soc. Japan, 43 (1970) 2727.
35. M. Gideon, M. Steiberg, J. Solid State Chem., 4 (1972) 370.
36. M. Che, J.F.J. Kibblewhite, A.J. Tench, M.Dufaux, C. Naccache, J.C.S. Faraday Trans. I, 69 (1973) 857.
37. A.S. Sass, V.A. Shvets, G.A. Savel'eva, N.M. Popova, V.B. Kazanskii, Kinet. Katal., 26 (1985) 924.
38. J. Soria, J.M. Coronado, J.C. Conesa, J.C.S. Faraday Trans. I, 92 (1996) 1619.
39. Ch.-A. Jenkins, D.M. Murphy, J. Phys. Chem. B, 103 (1999) 1019.
40. G. Li, X. Wang, X. Guo, S. Liu, Q. Zhao, Z. Bao, L. Lin, Mater. Chem. And Phys., 71 (2001) 195.
41. R.B. Clarkson, S. McClellan, J. Phys. Chem., 82 (1978) 325.
42. J.E. Wertz, J.R. Bolton, "Electron Spin Resonance", McGraw-Hill, New York, 1972, p.289.
43. J.A.McMillan and B.Smaller, J.Chem.Phys., 35 (1961) 1698.
44. P.C.Leung and F.Aubke, Inorg.Chem., 17 (1978) 1765.
45. P.C.Leung, K.C.Lee and F.Aubke, Can.J.Chem., 57 (1979) 326.
46. G.C.Allen and R.F.McMeeking, J.C.S.Dalton, (1976) 1063.
47. G.C.Allen, R.F.McMeeking, R.Hoppe and B.Muller, J.C.S.Chem. Comm., (1972) 291.
48. F.Holuj, J.Magn.Reson., 51 (1983) 37.
49. T.Miyanaga, K.Kan'no, S.Naoé and H.Matsumoto, J.Phys.Soc.Japan, 30 (1971) 1669.
50. N.Kanzaki and I Yasumori, J.Phys.Chem., 82 (1978) 2351.
51. N.M. Atherton, Electron Spin Resonance", Wiley, London, 1973, p.197.

52. C. Linke, M. Jansen, J. Solid State Chem., 134 (1997) 17.

53. J.A. McMillan, Chem. Rev., 62 (1962) 65.

54. W. Wang, H. Zhang, G. Lin, Z. Xiong, Appl. Catal., B: Environmental, 24 (2000) 219.

55. B. Kucharczyk, W. Tylus, Catal. Today, 90 (2004) 121.

Table 1

Some relevant characteristics of the catalysts prepared and tested

Catalyst	Nominal Composition	S_{BET} (m^2/g)	Min-max particle size (nm)
SGC-1	$SrTiO_3$	1	30-100
SGC-3	$SrTiO_3$	28	30-100
AgSGC-1	$Sr_{0.9}Ag_{0.1}TiO_3$	21	30-100
AgSGC-2.5	$Sr_{0.9}Ag_{0.1}TiO_3$	22	30-100
AgSGC-5	$Sr_{0.9}Ag_{0.1}TiO_3$	24	30-100
AgFH	$Sr_{0.9}Ag_{0.1}TiO_3$	12	50-800
FP	$SrTiO_3$	107	30-60
AgFP	$Sr_{0.9}Ag_{0.1}TiO_3$	67	30-60

FIGURE CAPTIONS

Fig.1 – XRD patterns of the various catalysts. (*a*) to (*h*): SGC-1, SGC-3, AgSGC-1, AgSGC-2.5, AgSGC-5, AgFH, FP, AgFP, in the order. All the patterns have been normalised as I/I_0. I_0 values (counts): (*a*) 1800, (*b*) 6280, (*c*) 6590, (*d*) 6000, (*e*) 6100, (*f*) 600, (*g*) 2850, (*h*) 2750.

Fig.2 – Comparison between the enlarged XRD patterns of SGC-1, AgFH, AgFP and AgSGC-1 catalysts. Upper part: main reflection (I_0); lower part: reflection at 2θ around 50°.

Fig.3 – Typical SEM micrographs of the various catalysts. (*a*) to (*h*): SGC-1, SGC-3, AgSGC-1, AgSGC-2.5, AgSGC-5, AgFH, FP, AgFP, in the order.

Fig.4 – Simplified scheme of the energy levels for the O_2^- ion in the presence of a crystal field.

Fig.5 - Comparison of EPR spectra (at 290 K) of AgSGC-5, AgFH and AgFP samples. Thinner tracks: patterns simulated by means of the equations suggested in [27].

Fig.6 – EPR spectra of AgSGC-1 and AgSGC-5 catalysts.

Fig.7 – Catalytic activity of the various catalysts.

Fig.8 – EPR spectra of (*a*) AgSGC-2.5R and (*b*) AgSGC-2.5 samples.

Fig.9 – Comparison of catalytic activity of AgSGC-2.5 and AgSGC-2.5R samples.

Fig.10 – Resistance to decaying of the catalysts prepared by the FP method.

Fig.11 – Resistance to decaying of the catalysts prepared by the FH method.

Fig.12 – Resistance to decaying of the catalysts prepared by the SGC method.

Fig.13 – Comparison of resistance to decaying of the AgSGC-2.5 and AgSGC-2.5R catalysts.

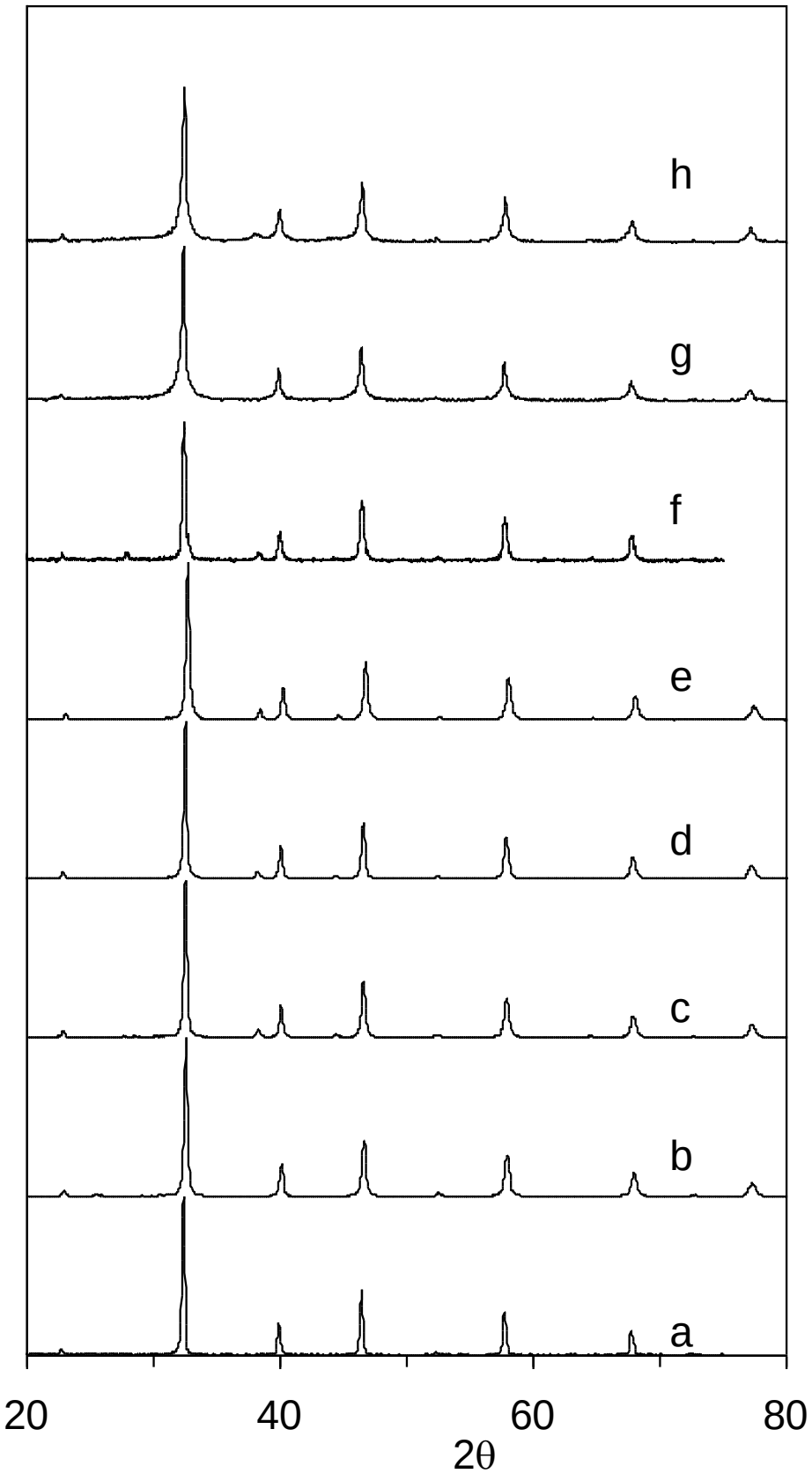

Fig. 1

Fig. 2

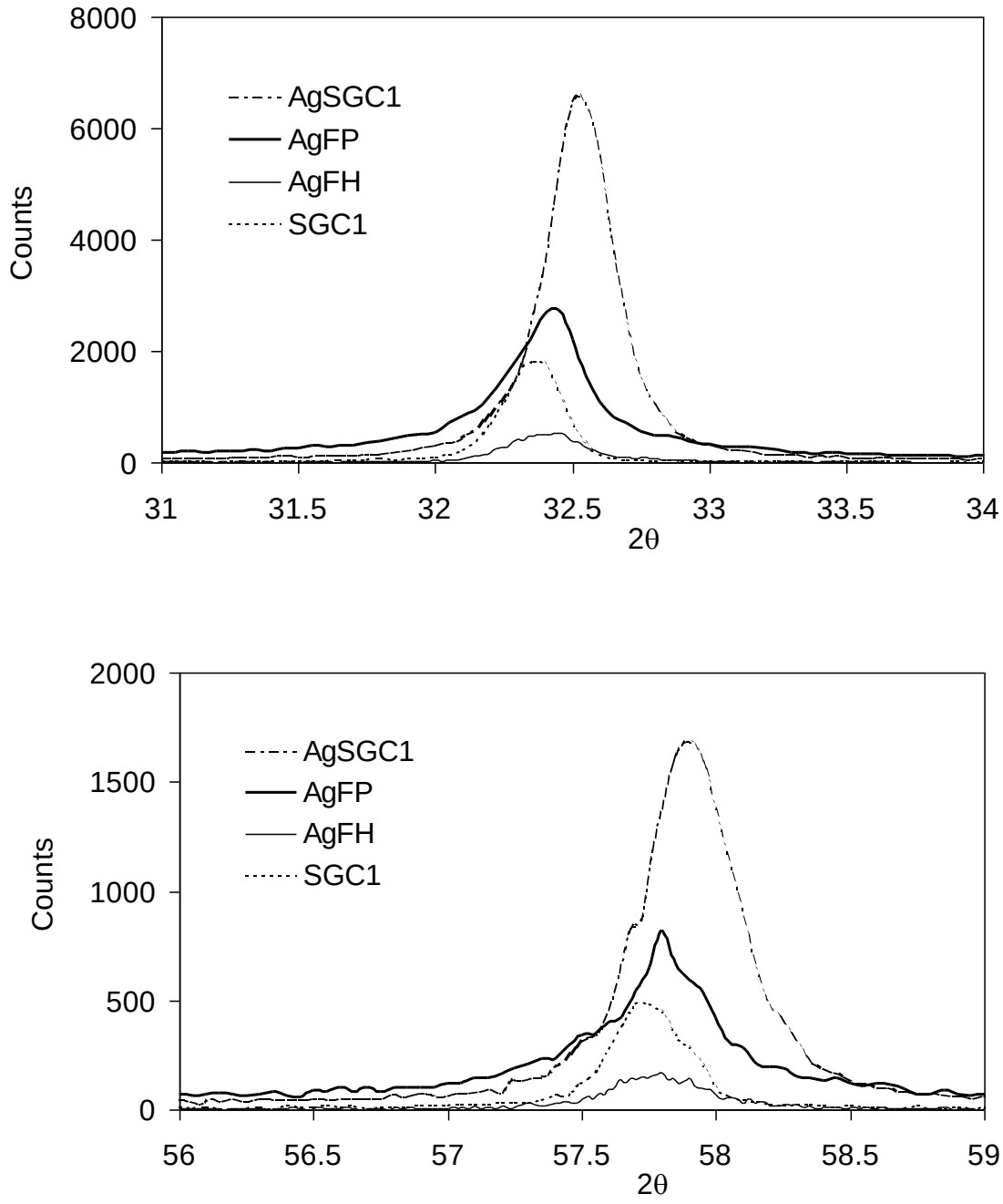
8000
6000
4000
2000
0
Counts
AgSGC1
AgFP
AgFH
SGC1
31
31.5
32
32.5
33
33.5
34
2θ
2000
1500
1000
500
0
Counts
AgSGC1
AgFP
AgFH
SGC1
56
56.5
57
57.5
58
58.5
59
2θ

Fig. 3

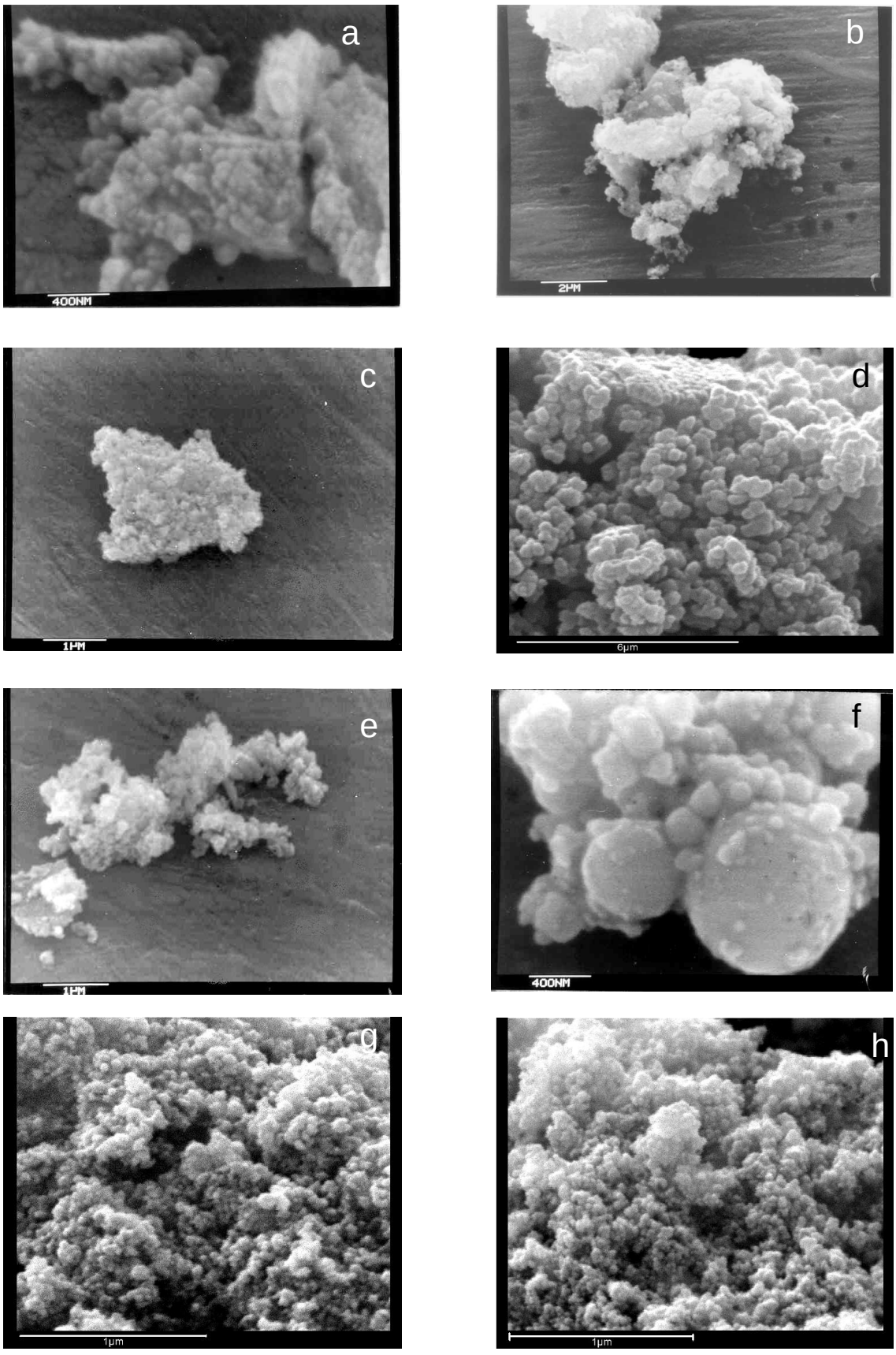

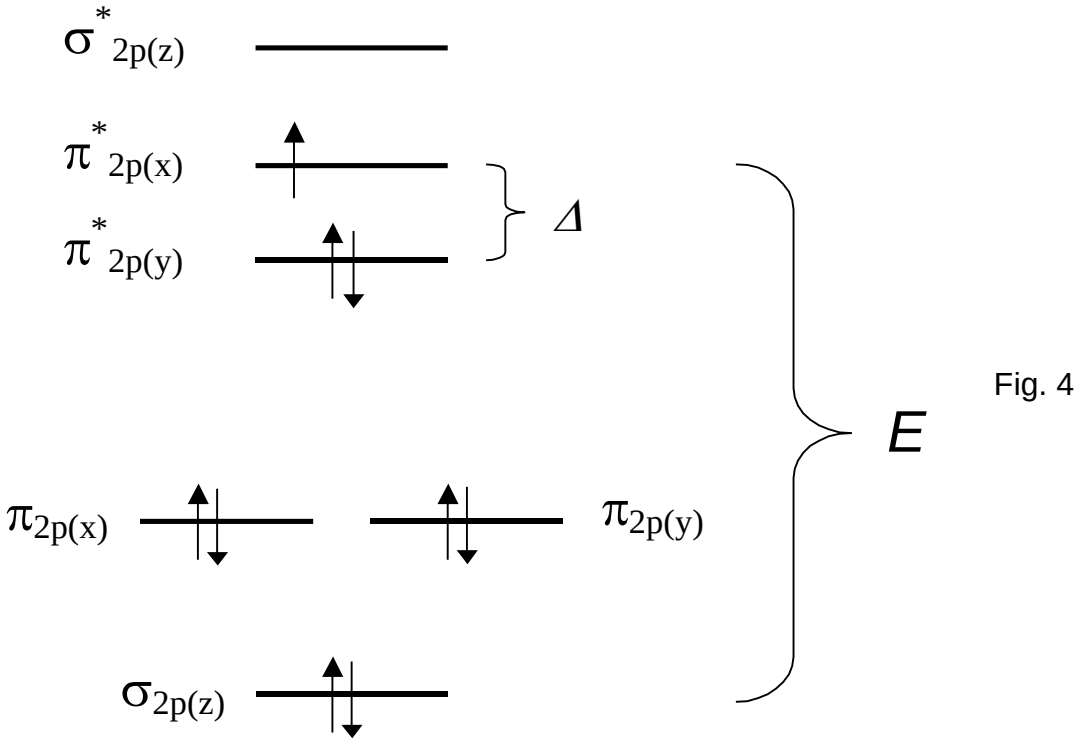

Fig. 4

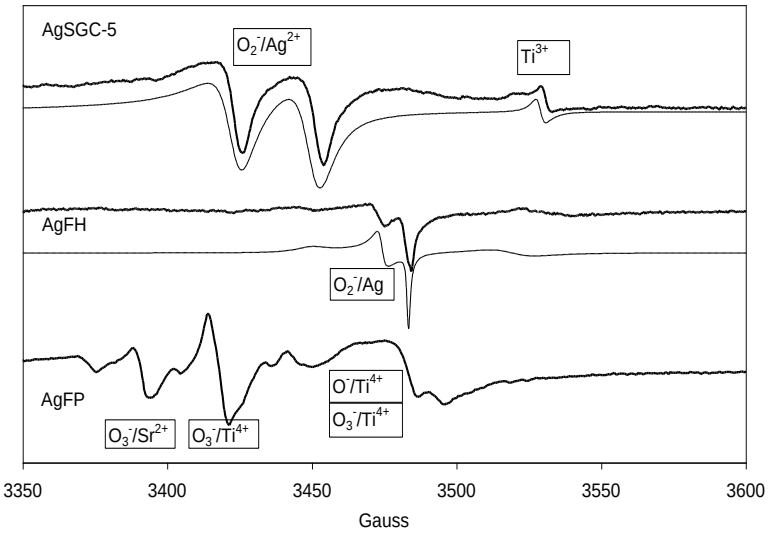
AgSGC-5
O_2^-/Ag^{2+}
Ti^{3+}
AgFH
O_2^-/Ag
AgFP
O^-/Ti^{4+}
O_3^-/Ti^{4+}
O_3^-/Sr^{2+}
O_3^-/Ti^{4+}
3350
3400
3450
3500
3550
3600
Gauss

Fig. 5

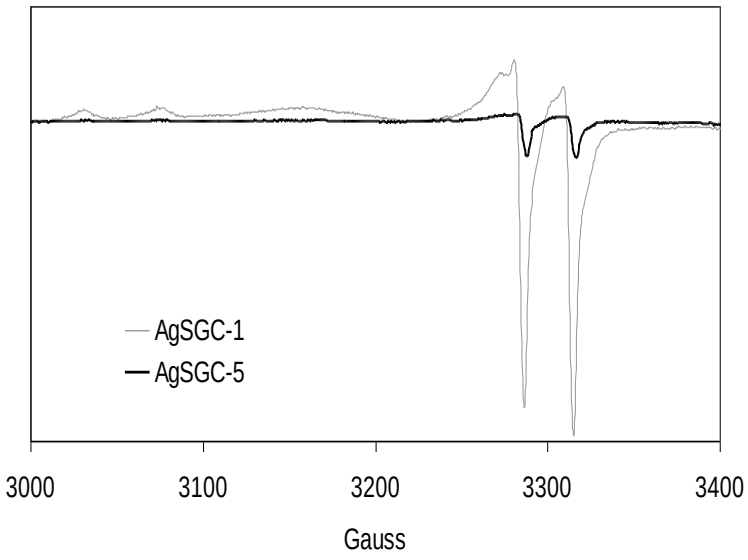
AgSGC-1
AgSGC-5
3000
3100
3200
3300
3400
Gauss

Fig. 6

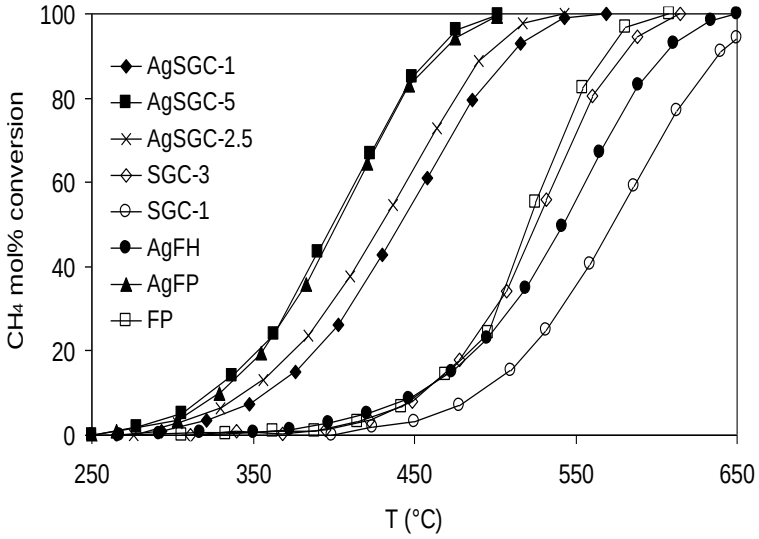
100
80
60
40
20
0
CH4 mol% conversion
AgSGC-1
AgSGC-5
AgSGC-2.5
SGC-3
SGC-1
AgFH
AgFP
FP
250
350
450
550
650
T (°C)

Fig. 7

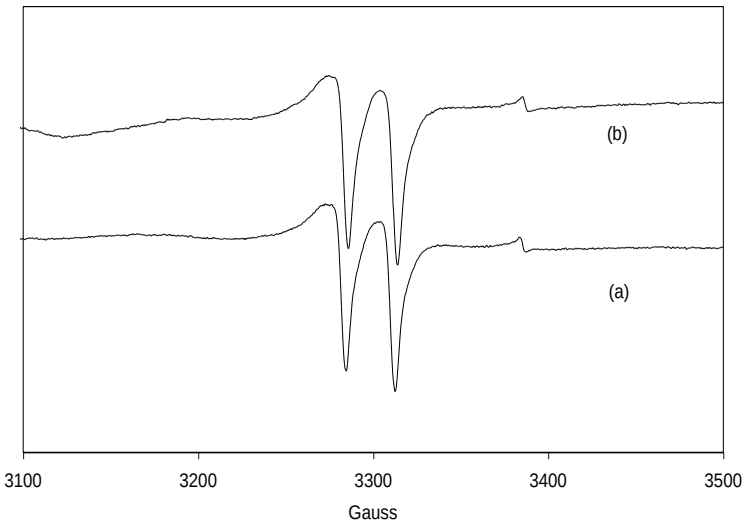
(b)
(a)
3100
3200
3300
3400
3500
Gauss

Fig. 8

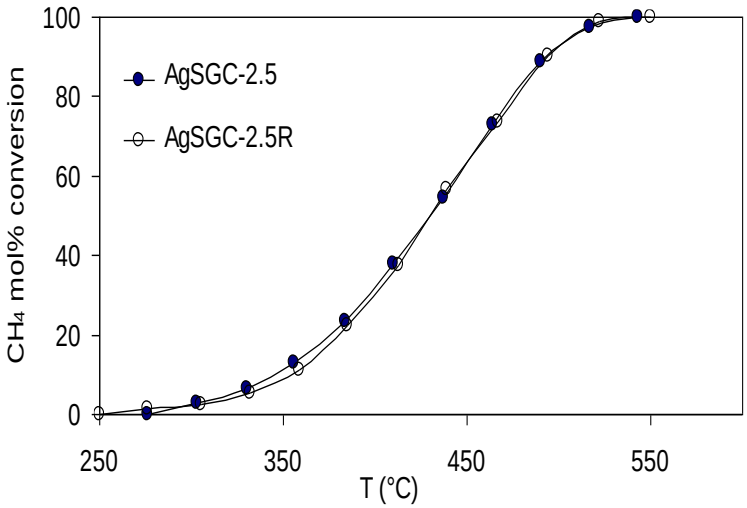
100
80
60
40
20
0
CH4 mol% conversion
AgSGC-2.5
AgSGC-2.5R
250
350
450
550
T (°C)

Fig. 9

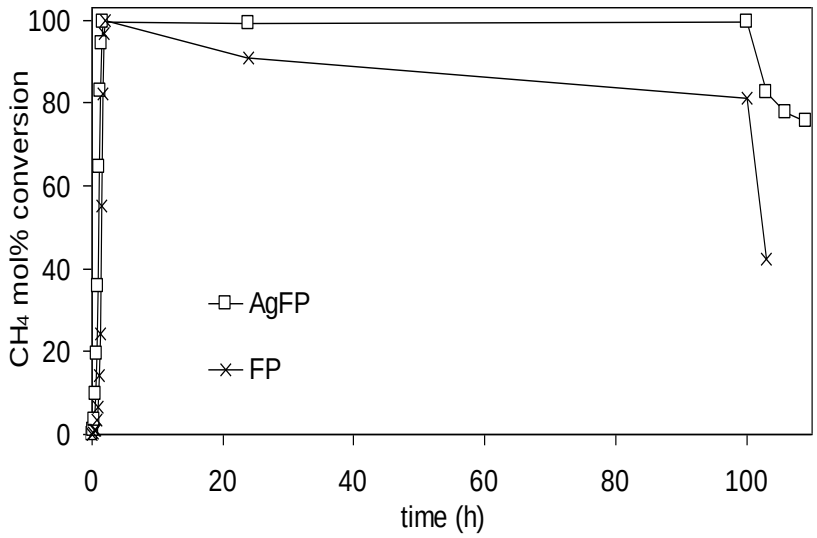
100
80
60
40
20
0
CH4 mol% conversion
0
20
40
60
80
100
time (h)
AgFP
FP

Fig. 10

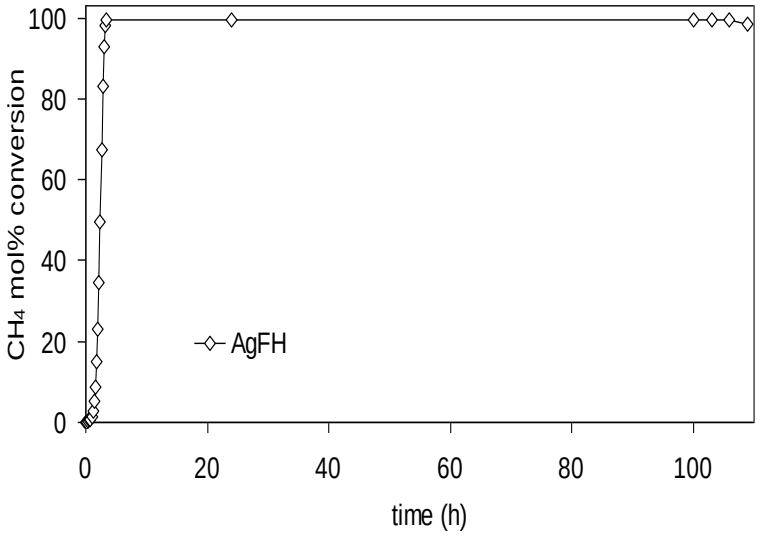
100
80
60
40
20
0
CH4 mol% conversion
0
20
40
60
80
100
time (h)
AgFH

Fig. 11

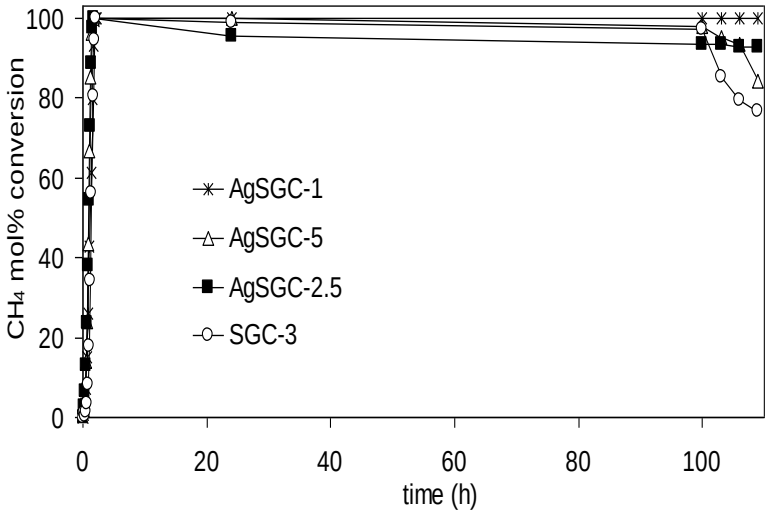
100
80
60
40
20
0
CH4 mol% conversion
AgSGC-1
AgSGC-5
AgSGC-2.5
SGC-3
0
20
40
60
80
100
time (h)

Fig. 12

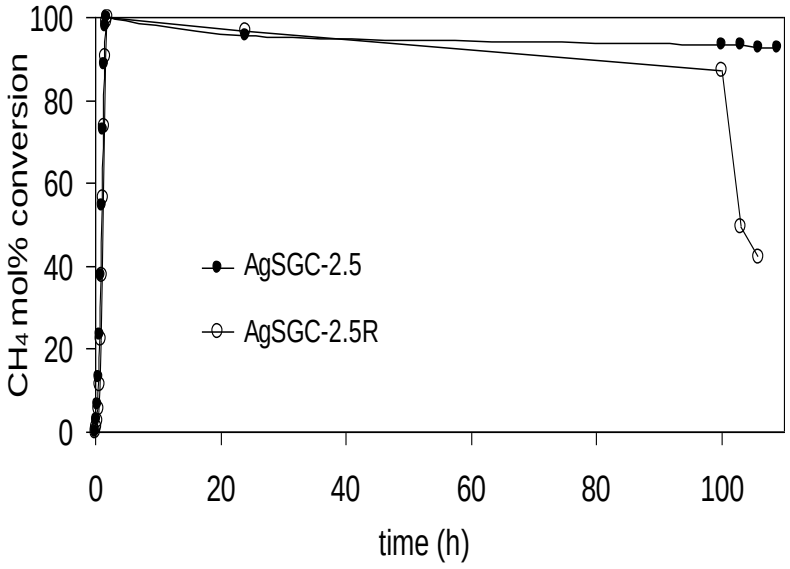
100
80
60
40
20
0
CH4 mol% conversion
AgSGC-2.5
AgSGC-2.5R
0
20
40
60
80
100
time (h)

Fig. 13